Journal Name

ARTICLE TYPE

Cite this: DOI: 00.0000/xxxxxxxxxx

Designing molecules with high-spin (quintet, $S = 2$) ground state for magnetic and spintronic applications†

Md Abdus Sabuj, Chinmoy Saha, Md Masrul Huda, and Neeraj Rai*

Received Date
Accepted Date

DOI: 00.0000/xxxxxxxxxx

High-spin ground-state polyradicals are an important platform due to their potential applications in magnetic and spintronic devices. However, a low high-to-low spin energy gap limits the population of the high-spin state, precluding their application at room temperature. Also, design strategies delineating control of the ground electronic state from closed-shell low-spin to open-shell polyradical character with the high-spin ground state are not well established. Here, we report indacenodinaphthothiophene isomers fused with 6,6-dicyanofulvene group showing a high-spin quintet ground state. Density functional theory calculations indicate the *syn*- and *anti*-configurations have a closed-shell low-spin singlet ground state. However, the *linear*-configuration displays a high-spin quintet ground state, with the energy difference between the high-spin quintet to the nearest low-spin excited states calculated as large as 0.24 eV ($\approx$ 5.60 kcal mol^{-1}), exhibiting an exclusive population of high-spin quintet state at the room temperature. These molecules are compelling synthetic targets for use in magnetic and spintronic applications.

0.0.0.1 Design, System, Application High-spin organic materials, where the ground electronic state possesses two or more unpaired electrons with parallel spins, are technologically relevant in organic magnetic and spintronic applications. Most organic materials exclusively have a low-spin singlet ground state, with a large energy of spin pairing. The challenge in the design and synthesis of high-spin state materials is to overcome this large energy of spin pairing in the singlet state to generate unpaired electrons, which is also persistent at ambient conditions. One approach could be to embed electron-deficient units into the molecular backbone so that recovery of aromatic stabilization energy can provide the necessary potential to break double bonds to generate multiple unpaired electrons. In this work, we have used a strong electron-withdrawing 6,6-dicyanofulvene group fused at the two opposite ends of indacenodinaphthothiophene isomers. Recovery of aromatic stabilization energy on the naphthothiophenes produces high-spin quintet ground-state for the *linear*-configuration, which are synthetic targets for room temperature magnetic applications.

* *Dave C. Swalm School of Chemical Engineering, and Center for Advanced Vehicular Systems, Mississippi State University, Mississippi State, Mississippi, USA 39762. Fax: +1 662 325 2482; Tel: +1 662 325 0790; E-mail: neerajrai@che.msstate.edu*

† Electronic Supplementary Information (ESI) available: [Computed electronic properties with different functionals, Optimized ground-state geometric parameters, HOMA values, NICS-XY values, MO diagrams, FOD plots, and AICD diagrams are provided in the supporting information.]. See DOI: 00.0000/00000000.

1 Introduction

High-spin (total spin quantum number, $S > 1$) ground-state open-shell polyradicals have drawn significant interest due to their potential applications in magnetic[1,2] and spintronic devices.[3,4] The weakly interacting unpaired electrons in the high-spin polyradical materials impart more exotic electronic, magnetic, and excited-state properties than their counterpart low-spin closed-shell materials. Also, an increased number of unpaired electrons in the high-spin polyradicals can provide the opportunity to investigate multiple spin–spin interactions,[5] which may facilitate the development of new magnetic devices.[1] Even though the high-spin ground-state polyradicals have great promises for next-generation magnetic-based materials and devices, scarcity of high-spin polyradicals with a large energy gap between the high-spin state to low-spin excited state precludes their potential application as room temperature magnetic materials.

If the materials possess more than two unpaired spins, bulk magnetic properties in organic semiconductors (OSCs) can be realized.[6] Moreover, the characteristic energy difference between the high-spin ground-state to low-spin excited state needs to be larger than 1.0 kcal mol^{-1}, sufficiently surpassing the room temperature thermal energy, RT.[1,2,7] Prototypical classes of high-spin polyradicals are developed using 'spin-centers' which are connected by ferromagnetic coupling units (FCUs). (see Fig. 1a–c)[1,7–11] By utilizing this approach, high-spin polyradicals have been developed, where the spin quantum number is extended to $S = 5000$.[12] However, lack of π-conjugation and highly localized bonding induce spin ordering at a very low temperature (< 10.0

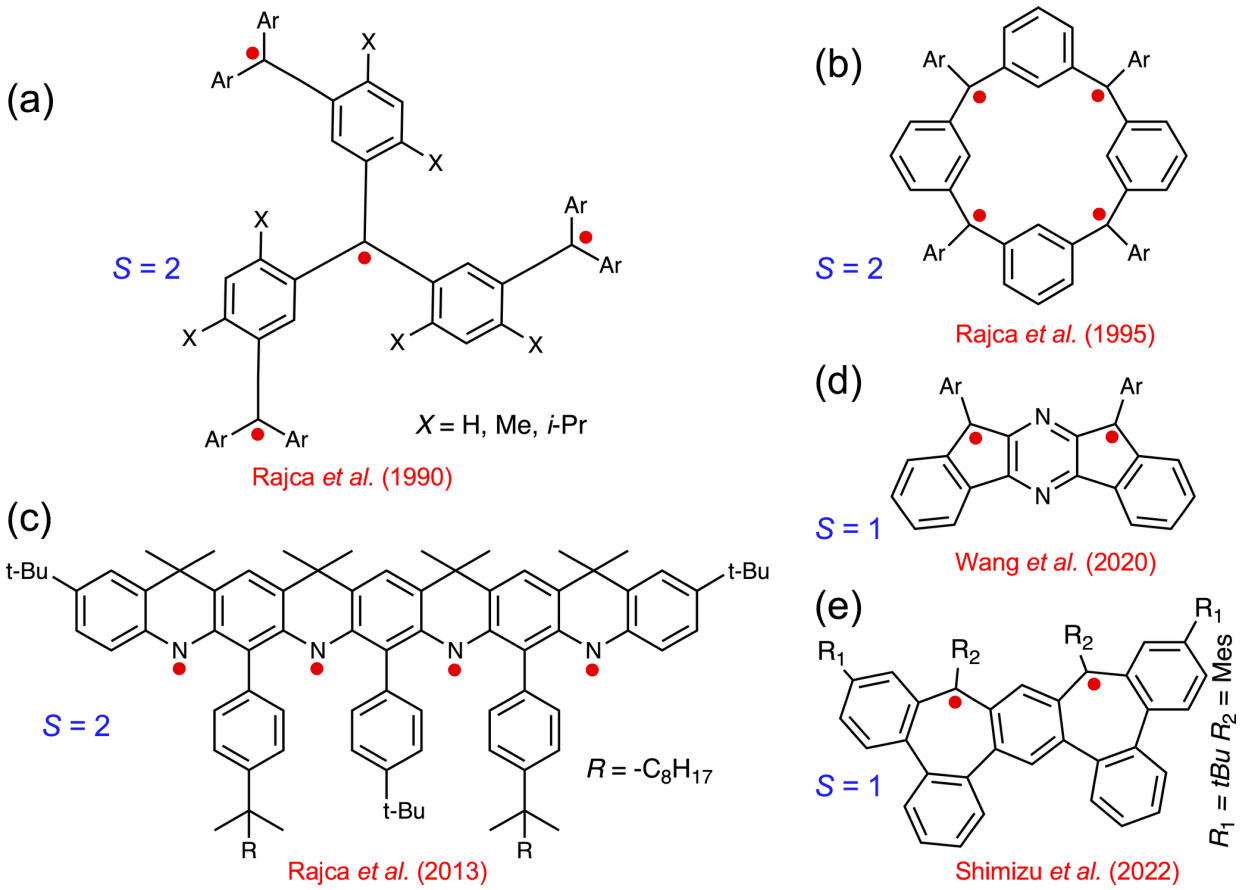

Fig. 1 Prototypical classes of high-spin state organic materials showing quintet ($S = 2$) (a–c) and triplet ($S = 1$) (d–e) ground-state.

K). Recent works on donor-acceptor (D-A) type polymers promote large π-conjugation and small band gap, generating high-spin triplet ($S = 1$) ground-state, with a small singlet–triplet energy gap ($\Delta E_{ST} << RT$).[13–22]

Open-shell OSCs based on polycyclic hydrocarbons (PCHs)[23–25] possess a highly conjugated, rigid, and planar molecular backbone. These small molecules are easy to synthesize and eliminate the complexities due to impurities and structural heterogeneity, which gives these materials an edge over large polymers. As a result, PCHs act as a holy grail for developing open-shell molecules with interesting electronic and magnetic properties. However, the majority of the PCHs (with or without substituted heteroatoms) have a small-to-moderate open-shell character and possess a singlet ($S = 0$) ground-state due to the double-spin polarization[26] with low-lying triplet excited state.[5,25,27–42] Recent studies on high-spin substituted PCHs report a triplet ($S = 1$) ground-state (Fig. 1d–e), showing the possibilities to design hydrocarbon-based materials with magnetic properties.[43,44]

Haley and co-workers have introduced an interesting strategy to modulate the electronic properties of the substituted PCHs by incorporating *s*-indacene at the core fused with carbo-cycles and hetero-cycles.[30,31,40] The π-conjugated *s*-indacene has a large antiaromatic character (12 π-electrons) with a C_{2h} symmetry and is highly unstable.[32,45] Optimization of *s*-indacene's molecular structure and properties involved the substitution of bulky *tert*-butyl groups to kinetically block the reactive sites[46] or fusion of external five-/six-membered rings to extend the π-conjugation path served as the most proficient strategies.[30–32,34,40,47–49] The fusion of external rings modulates the paratropicity of the *s*-indacene core, reducing the highest occupied molecular orbital (HOMO)–lowest unoccupied molecular orbital (LUMO) energy gap.[31,32,40] Our recent study[50], where we have thoroughly investigated the relationship between HOMO–LUMO energy gap and open-shell character, show molecules with a smaller HOMO–LUMO energy gap provide more open-shell character. This is due to the fact that, a small energy gap facilitates admixing of the frontier MO (FMO) into the ground-state, generating open-shell character.[51] Open-shell character of the molecules with *s*-indacene core indicates a moderate diradical character, obtained at the spin-projected unrestricted Hartree-Fock (PUHF) method (see Table S1).[34] Due to a large spin-contamination inherent to the PUHF method, the open-shell diradical character obtained is largely overestimated.[50,52] Therefore, the electronic ground-state of the available materials with *s*-indacene core lies in between the closed-shell and open-shell low-spin singlet state, with a thermally accessible high-spin triplet excited state.[34,40,49]

Here, we report end-group functionalized naphthothiophene-fused *s*-indacene isomers (Fig. 2 and Fig. S1) with a high-spin quintet ($S = 2$) ground state. For the end-group functionalization, we have used 6,6-dicyanofulvene group substituted at the ends of the naphthothiophenes. Substitution of the strong

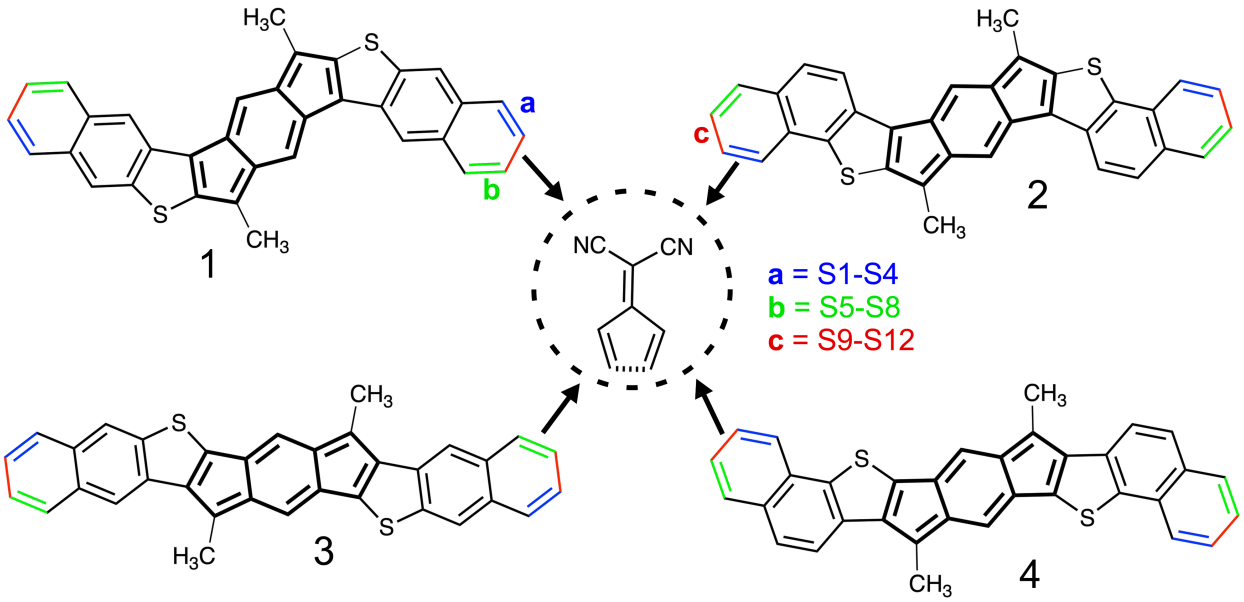

Fig. 2 Indacenodinaphthothiophene isomers (**1**–**4**) with a large antiaromatic core.[32] 6,6-dicyanofulvene group substituted indacenodinaphthothiophene isomers with closed-shell singlet state (**S1**–**S8**) and open-shell quintet state (**S9**–**S12**) studied in this work. *a*, *b*, and *c* are the locations on the outer benzene rings where the 6,6-dicyanofulvene group is substituted. If the sulfur of the thiophene ring and substituents are on the same side (**a** position), molecules are termed as *syn*-isomer (**S1**–**S4**), else, molecules are termed as *anti*-isomer (**b** position, **S5**–**S8**). When substitutions are made along the molecular backbone (**c** position), these molecules are termed as *linear*-isomer (**S9**–**S12**). Detailed diagrams of the molecular structures are also can be found in the Supporting Information (see Fig. S1).

electron-withdrawing dicyanomethylene groups can downshift the LUMO energy level, reducing the FMO energy gap, and generating open-shell character.[53–59] On the other hand, the addition of the five-membered carbonaceous rings can modulate the aromatic character along the molecular backbone, generating an open-shell polyradical character.[60–64] Although, there is a significant amount of work available on molecular-based diradicals,[5,14,16–19,27–29,33,34,36–38,50,51,55,65–67] very few studies report open-shell materials with a large polyradical character.[60–64,68–73] In the open-shell diradicaloid form, the benzenoid ring at the *s*-indacene core can regain aromatic stabilization energy at the expense of the double-bond breaking of the dicyanomethylene groups (Fig. 3ii). However, as the *s*-indacene core has a very high antiaromatic character, in the most stable configuration, the naphthothiophenes can recover aromatic stabilization energy in the tetraradicaloid state (Fig. 3iii–iv). This study establishes design strategy for developing substituted PCHs into high-spin polyradicals suitable for magnetic and spintronic applications.

2 Computational details

Geometry optimizations are performed with Gaussian 16 software package[74] at the C_{2h} symmetry using hybrid density functional B3LYP[75,76], and 6-31G(d,p)[77] basis set. Frequency calculations confirm the local minima of all the molecules. All parameters for geometry optimizations are set to default. Unless otherwise specified, analyses are performed with (U)B3LYP level of theory. B3LYP has been used extensively for molecules with open-shell character, and generally there is good agreement with experimental geometric parameters, such as bond lengths.[27,50,78] The high-to-low spin energy gap calculated with (U)B3LYP method was found to agree with the experimental observation.[11,78,79] Our study on polymeric material predicted a high-spin ground state with (U)B3LYP functional for larger repeat units, which is also verified with experimental data.[16] A more detailed discussion on different functionals can be found in Ref. 18.

A broken-symmetry (BS)[80] wave function is used to characterize the open-shell singlet state. The contribution of the open-shell character is quantified with the multi-radical indexes, y_i ($i = 0$–2), where $y_i = 0$ indicate a closed-shell configuration, and $y_i = 1$ dictates a pure open-shell structure.[51]. The triplet and quintet states are optimized with an unrestricted wave function and the wave functions are optimized if instability was observed. The triplet–quintet energy gap (ΔE_{TQ}) of the open-shell molecules are computed with the following equation, which adds correction for spin contamination.[11]

$$\Delta E_{TQ} = \Delta E_{UHF} \frac{< S^2_Q > -2.0}{< S^2_Q > - < S^2_T >} \quad (1)$$

where, ΔE_{UHF} is the uncorrected energy difference between the ground-state quintet and triplet states, and $< S^2_Q >$ and $< S^2_T >$ are the expectation values of the spins for the quintet and triplet states, respectively.

The locations of the unpaired spins are predicted with the NBO7 program package[81]. Nucleus independent chemical shift (NICS)-XY[82,83] scan and $NICS_{ZZ}$ are computed with the gauge-independent atomic orbital (GIAO)[84] method at 1.7 Å above the plane of the rings, where a large positive NICS value is an indication of an antiaromatic structure and negative values show aromatic configuration. The $NICS_{iso}(1)$ of the isolated substituents are computed at 1.0 Å above the rings plane. Anisotropy of the

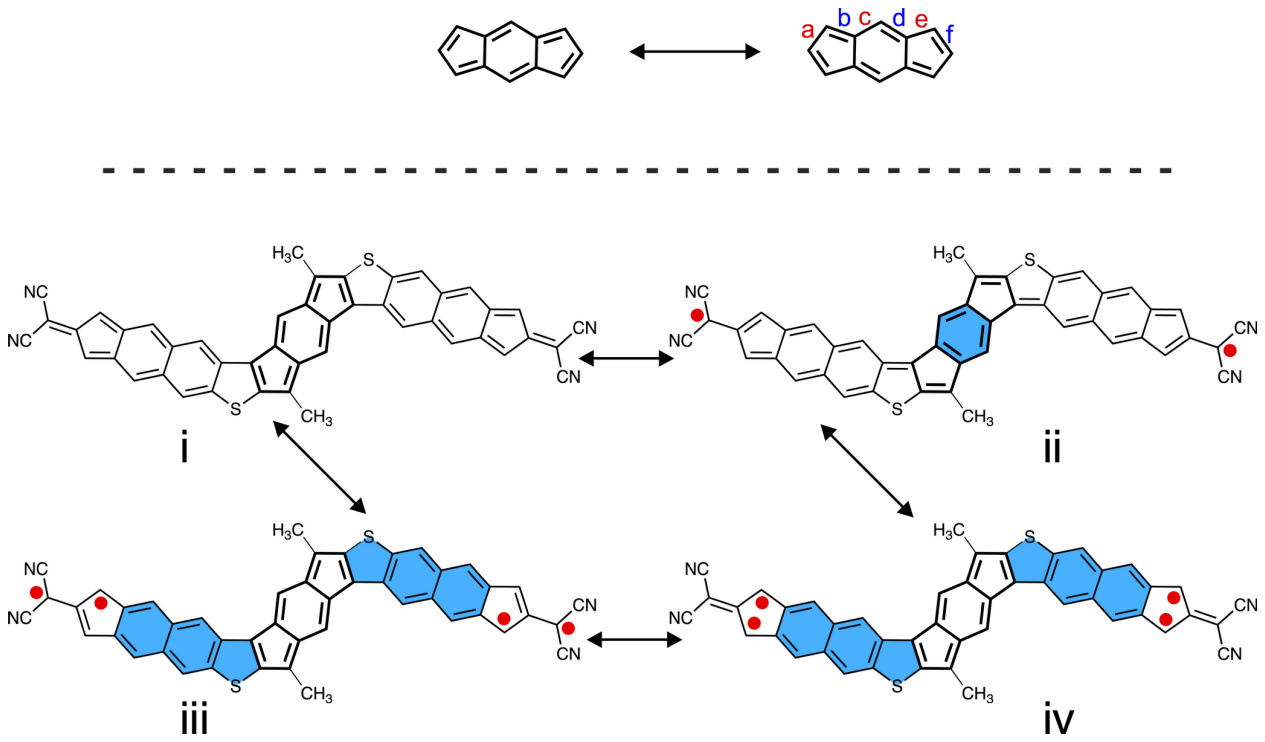

Fig. 3 Resonance diagrams of *s*-indacene at the C_{2h} symmetry (top) and resonance diagrams (i–iv) of **S9** showing the development of polyradical character. Recovery of aromatic stabilization energy in the sulfur-containing five-member rings, and the benzenoid rings provides the potential energy required to break double-bonds.

induced current density (ACID) method[85] at CSGT-(U)B3LYP/6-31G(d,p) level of theory[86] is used to generate the ring current density, and rendering is performed with a locally developed code. The 2D-iso-chemical shielding surface (2D-ICSS) maps are generated by the method developed by Klod *et al.*[87] The fractional occupation number weighted electron density (N_{FOD})[88] is calculated with the ORCA[89] program package. The harmonic oscillator model of aromaticity (HOMA)[90] is calculated with:

$$HOMA = 1 - \frac{98.89}{n}\sum_{i=1}^{n}(R_i - 1.397)^2 \qquad (2)$$

where, n is the number of bonds considered in a particular ring, R_i is the optimized bond length at the equilibrium geometry. HOMA = 1 indicates an aromatic structure.[90,91] Molecular orbital diagrams and spin density plots are generated with the VMD.[92]

3 Results and Discussion

3.1 Selection of the parent molecules and different substituents

We have selected the naphthothiophene-fused *s*-indacene isomers (**1–4** in Fig. 2) as these molecules possess the lowest HOMO–LUMO energy gap reported on *s*-indacene derivatives.[32,34] A small HOMO–LUMO gap can admix the frontier MOs into the ground state, generating an open-shell character.[16,50,65,68] Also, a small FMO gap reduces the energy difference between the high-to-low spin state, which is required for magnetic switching from low-spin state to high-spin state.[16,18,21,36,68] Furthermore, due to a large antiaromatic *s*-indacene core, these molecules are good candidates for developing open-shell configurations. Indeed, previous reports on similar materials show moderate open-shell diradical character obtained at the PUHF level of theory.[33,34] Our calculations with the PUHF method on the parent molecules (**1–4** in Fig. 2) also indicate these isomers possess small diradical character (see Table S1). However, the conventional density functional theory (DFT) method combined with the broken-symmetry (BS) approach does not provide an open-shell character. This indicates that the PUHF method overestimates the open-shell character due to its large spin contamination (Table S2).[50,52] Therefore, we have used the BS-DFT method to characterize the open-shell polyradical character, where the open-shell and closed-shell molecules are identified according to the polyradical index, y_i (i = 0–2). Such as $y_i = 0$ indicates a closed-shell configuration, and $y_i = 1$ dictates a pure open-shell structure, respectively.

The 6,6-dicyanofulvene group used for the end-functionalization selected from a computational screening of different substituents (see Fig. S2). Our target was to find molecules with a large open-shell diradical or polyradical character. We find that the external five-membered ring fused with the indacenodinaphthothiophene is the key to obtaining open-shell character (Fig. 4 and Table S3–S4). Such as the mere addition of CN groups into the isomer **1** and **2** did not produce an open-shell electronic configuration (**S13** in Fig. 4 and Table S3, **S19** in Table S4). However, the addition of the carbon-containing five-membered ring develops open-shell character (**S14–S18** in Fig. 4 and Table S3, **S20–S24** in Table S4). Substitution of the different functional groups with the carbon

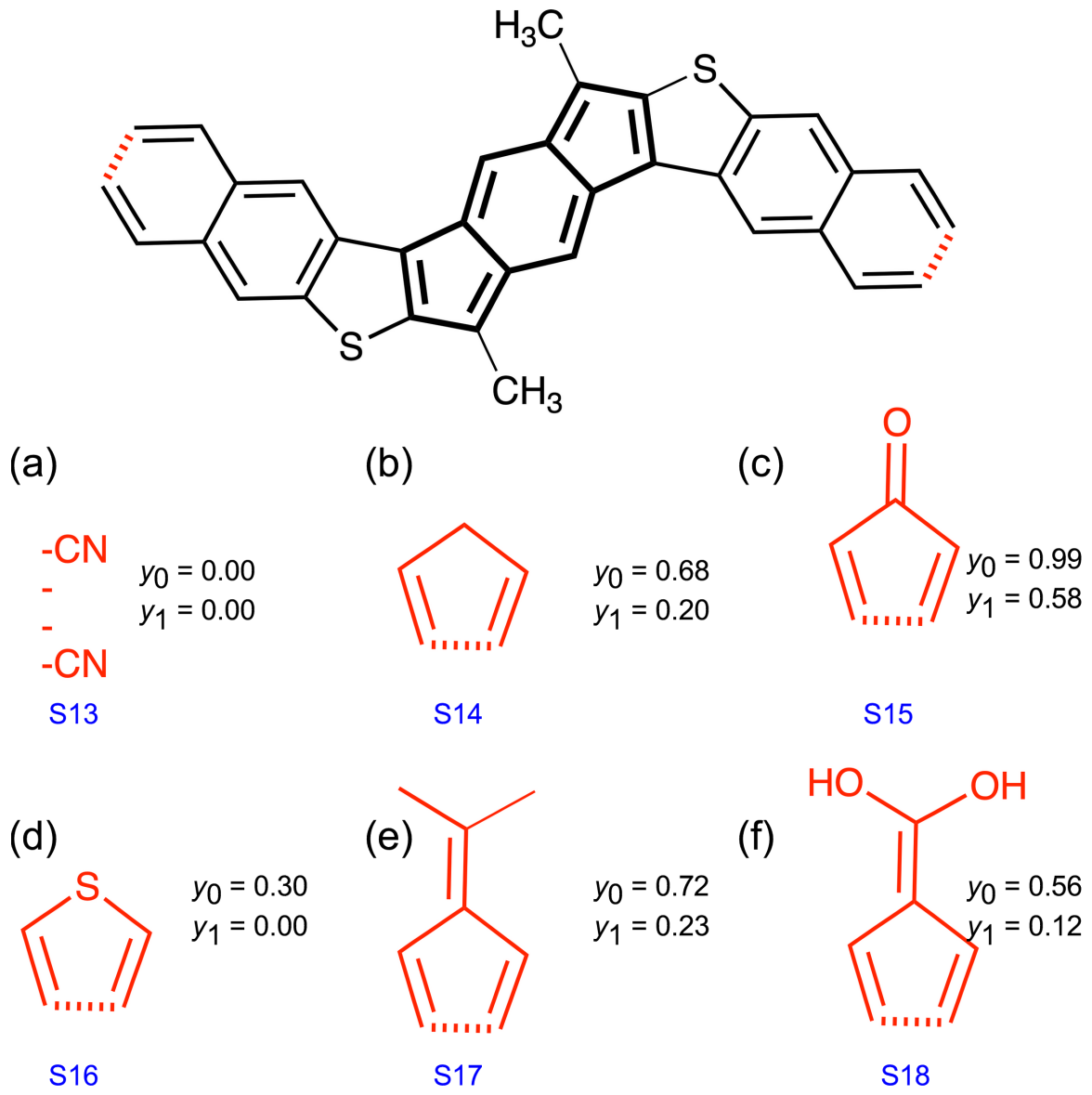

Fig. 4 Modulation of the molecular topology tunes the electronic properties of the high-spin polyradicals.

rings modulates low-to-high spin energy gap, HOMO–LUMO gap, and open-shell polyradical character (see Table S3 and S4). The largest open-shell polyradical character is obtained when the dicyanomethylene groups are attached to the carbon-containing five-membered carbonaceous rings. Also, it is reported that a strong electron withdrawing group can generate high-spin materials.[43] Therefore, we have used different substituents with increasing acceptor strength, indicated by a more downshifted LUMO energy levels and increasing $NICS_{iso}(1)$ values (Fig. S2). The 6,6-dicyanofulvene group has the lowest LUMO energy levels among the different substituents used in this study. As a result, the 6,6-dicyanofulvene group substituted molecules produce a high-spin quintet ($S = 2$) state. Therefore, the 6,6-dicyanofulvene group substituents are subjected to further in-depth analysis. Also, different locations of the substituents on the naphthothiophenes modulate the ground-state from closed-shell singlet to open-shell high-spin polyradicals. Such as substitutions on the **a** (isomers **S1**–**S4**, *syn*-configurations) and **b** (isomers **S5**–**S8**, *anti*-configurations) bonds (see Fig. 2) produce closed-shell singlet ground-state. Only substitution on the **c** (isomers **S9**–**S12**, *linear*-configurations) bond develops open-shell polyradical character with a high-spin $S = 2$ ground-state observed on isomers **S10**–**S12**. This study indicates easy tuning of electronic properties by simple topological modifications on the available molecular frameworks.

3.2 Ground-state structure and geometric parameters

Bond lengths are analyzed to get insight into the geometries and aromatic/antiaromatic character of the parent and designed isomers (see Table 1 and Fig. S3–S6). Due to the antiaromatic nature of the *s*-indacene core, it possesses a large bond length alternation (BLA).[32,34] A large BLA is observed in the **1**–**2** isomers; however, BLA is reduced in the **3**–**4** isomers. Addition of the 6,6-dicyanofulvene group produce a more pronounced BLA for the

Table 1 Bond lengths at the *s*-indacene core of the different isomers observed at the singlet ($S=0$) state. Bond indexes are provided in Fig. 3.

Isomer	Bond lengths (Å)					
	a	*b*	*c*	*d*	*e*	*f*
1	1.400	1.452	1.380	1.416	1.417	1.419
2	1.400	1.455	1.377	1.419	1.411	1.424
3	1.410	1.426	1.387	1.405	1.420	1.423
4	1.399	1.439	1.375	1.419	1.403	1.443
S1	1.398	1.457	1.372	1.424	1.405	1.432
S2	1.393	1.458	1.373	1.423	1.407	1.430
S3	1.405	1.434	1.378	1.416	1.406	1.439
S4	1.401	1.432	1.380	1.413	1.409	1.437
S5	1.397	1.456	1.373	1.423	1.405	1.432
S6	1.395	1.459	1.372	1.424	1.406	1.431
S7	1.403	1.435	1.378	1.416	1.406	1.439
S8	1.405	1.431	1.380	1.413	1.408	1.437
S9	1.416	1.452	1.389	1.405	1.441	1.400
S10	1.417	1.457	1.387	1.407	1.443	1.400
S11	1.412	1.428	1.386	1.407	1.418	1.428
S12	1.405	1.433	1.379	1.415	1.407	1.440

syn- (**S1**–**S4**) and *anti*-isomers (**S5**–**S8**). A larger BLA is an indication of a closed-shell quinoidal configuration, where the closed-shell form is in resonance with the open-shell configuration.[27] In the cases of the *linear*-isomers, BLA is reduced in the *s*-indacene core compared to the parent (**1**–**4**), *syn*-, and *anti*-isomers (Table 1). This indicates the *s*-indacene core of the *linear*-isomers reduces its large antiaromatic character to provide the potential for bond breaking, generating open-shell polyradical character. A mixed single and double bond indicates a large π-conjugation along the molecular backbones, which can reduce the HOMO–LUMO energy gap. The bond lengths (*e* in Fig. 3) from the apical carbon atom to the *s*-indacene core varies as 1.403–1.420 Å in the parent, 1.405–1.409 Å in the *syn*- and *anti*-isomers, whereas, a larger bond lengths (1.407–1.443 Å) are observed for the *linear*-isomers. It also indicates a large open-shell character in the *linear*-isomers than the other molecules.[27]

Substitution of the 6,6-dicyanofulvene group into the parent isomers leads to different bonding patterns. The bond lengths of the outer benzenoid ring for the parent isomers vary between 1.375–1.440 Å, indicating a more aromatic character (see Fig. S3). The calculated HOMA values of the outer benzenoid ring of the parent isomers are close to 1.0 (Fig. S7), which also shows their aromatic character. In the cases of the *syn*- and *anti*-isomers, bond length variation ranges between 1.360–1.500 Å (see Fig. S4–S5), indicating a more antiaromatic character than the parent isomers and have a closed-shell conformation. HOMA values of the outer benzenoid ring of the *syn*- and *anti*-isomers decreased significantly (≈ 0.65), confirming their more antiaromatic character than the parent isomers (see Fig. S8–S9). For the *linear*-isomers in the $S=2$ ground-state, the bond lengths of the double bonds have increased (1.42 Å), whereas the length of the fusion bonds between the carbonaceous ring and outer benzenoid ring have decreased (1.46 Å *vs.* 1.50 Å) than the *syn*- and *anti*-isomers (Fig. S4–S6). The calculated HOMA values of the outer benzenoid ring increased (≈ 0.90) more than the *syn*- and *anti*-isomers (Fig. S8–S10). These bond lengths and HOMA values indicate a lower antiaromatic character of the *linear*-isomers than the *syn*- and *anti*-isomers, respectively. A reduction of antiaromatic character provides the necessary potential for double bond breaking, generating open-shell polyradical character and stabilizing high-spin $S=2$ ground-state in the *linear*-isomers.

3.3 High-to-low spin energy gap of the parent and designed isomers

The ground electronic state of a molecule is correlated with the energy difference between the high-spin and low-spin states (ΔE_{LH}). Generally, the open-shell molecules possess a smaller ΔE_{LH} than the closed-shell molecules.[50,65] We have computed the energy difference between the singlet–triplet (ΔE_{ST}) and triplet–quintet (ΔE_{TQ}) states to determine the ground electronic state. All the electronic properties of the parent and designed isomers are provided in the Table 2. As we can see from Table 2, the parent molecules (**1**–**4**) have a large ΔE_{ST}, which shows that the parent molecules have a closed-shell electronic configuration with a triplet excited state. The computed ΔE_{TQ} of the parent molecules are significantly larger than the ΔE_{ST}, indicating a low-spin singlet ground-state. Substitution of the 6,6-dicyanofulvene group reduces both the ΔE_{ST} and ΔE_{TQ} gaps of the designed isomers (**S1**–**S12**) than the parent isomers, which indicates extension of the π-conjugation length reduces ΔE_{LH}. Furthermore, the open-shell isomers have a significantly smaller ΔE_{LH} than the closed-shell molecules. Such as, the largest ΔE_{ST} is observed for isomer **4** (0.947 eV) with a closed-shell configuration, whereas the **S10** with an open-shell character possesses the smallest singlet–triplet energy gap (0.05 eV).

The energy diagram of the **S9**–**S12** molecules indicate the singlet closed-shell (SCS) configuration is significantly higher in energy than the singlet open-shell (SOS) form (Fig. S11). This indicates the open-shell configuration is more stable in energy than the closed-shell. Such as, in reference to the quintet ($S=2$) state, the SOS state of the **S12** is 0.35 eV higher in energy. However, the energy difference between the SCS and $S=2$ states of **S12** is 0.88

Table 2 Computed electronic properties of the indacenodinaphthothiophene isomers at (U)B3LYP/6-31G(d,p) level of theory and basis set. The singlet–triplet energy gap ($\Delta E_{ST} = E_T - E_S$), triplet–quintet energy gap ($\Delta E_{TQ} = E_Q - E_T$), population ($P_Q$) of the quintet ($S = 2$) state at room temperature, energies of the highest occupied MO (HOMO) and the lowest unoccupied MO (LUMO), energetic difference between the FMOs (E_g), fractional occupation number weighted electron density (N_{FOD}), diradical (y_0), tetraradical (y_1), and hexaradical (y_2) character indexes of the molecules. Energy values are in eV, N_{FOD}, and y_i's are dimensionless quantities. For the closed-shell molecules (**1–4** and **S1–S8**) SCS and for the open-shell molecules (**S9–S12**) SOS energy was used for ΔE_{ST} calculation.

Isomers	ΔE_{ST}	ΔE_{TQ}	P_Q	HOMO	LUMO	E_g	N_{FOD}	y_0	y_1	y_2
1	0.541	2.559	0.00	−4.76	−3.15	1.61	2.29	0.000	0.000	0.000
2	0.499	2.957	0.00	−4.82	−2.97	1.85	2.12	0.000	0.000	0.000
3	0.950	1.991	0.00	−4.83	−2.87	1.96	2.12	0.000	0.000	0.000
4	0.947	2.124	0.00	−4.86	−2.78	2.08	2.00	0.000	0.000	0.000
S1	0.500	0.357	0.00	−5.55	−3.96	1.59	3.98	0.000	0.000	0.000
S2	0.433	0.184	0.00	−5.43	−4.01	1.42	4.00	0.000	0.000	0.000
S3	0.951	−0.163	99.85	−5.48	−3.83	1.65	3.94	0.000	0.000	0.000
S4	0.839	−0.185	99.91	−5.34	−3.86	1.48	3.98	0.000	0.000	0.000
S5	0.542	0.291	0.00	−5.45	−3.85	1.60	4.00	0.000	0.000	0.000
S6	0.383	0.250	0.00	−5.48	−4.07	1.41	4.02	0.000	0.000	0.000
S7	0.903	−0.147	99.73	−5.41	−3.82	1.59	3.95	0.000	0.000	0.000
S8	0.862	−0.220	99.98	−5.45	−3.91	1.54	3.98	0.000	0.000	0.000
S9	0.267	−0.282	100.00	−5.42	−4.02	1.40	5.64	0.986	0.776	0.122
S10	0.050	−0.365	100.00	−5.43	−4.08	1.35	5.40	0.937	0.556	0.111
S11	−0.167	−0.240	99.99	−5.39	−3.96	1.43	5.73	0.958	0.871	0.060
S12	−0.176	−0.240	99.99	−5.39	−4.01	1.38	5.59	0.928	0.800	0.030

eV, significantly higher than the SOS state. The SCS of the **S9–S12** isomers are 0.79 eV–1.09 eV higher in energy than the $S = 2$ state, indicating a large polyradical character inherent to these molecules (Fig. S11). The SOS state of the **S9** isomer is 0.05 eV lower in energy than the $S = 2$ state. This indicates the **S9** has an open-shell singlet ground-state with a thermally activated quintet ($S = 2$) state. Although, isomer **S9** has a singlet ground-state, **S10–S12** isomers show a $S = 2$ ground-state. The SOS state of the **S10** is above 0.24 eV from the reference $S = 2$ state, whereas, the triplet ($S = 1$) is above 0.37 eV from the ground-state, indicating the SOS is the thermally accessible excited state than the triplet state. In the cases of the **S11–S12** isomers, the triplet excited state is above 0.24 eV from the $S = 2$ ground-state. At this large ΔE_{TQ}, the population of the $S = 2$ state is 100 %, showing exclusive population of high-spin quintet state at room temperature. Calculations performed with CAM-B3LYP[93] and ωB97X-D[94] also indicate a large ΔE_{TQ} and $S = 2$ ground-state (see Table S2), indicating the high-spin quintet state is intrinsic to the *linear*-isomers. For the *syn*- and *anti*-isomers, the SOS and SCS are degenerate in energy, indicating a closed-shell low-spin singlet ground-state with a large ΔE_{ST}. However, the computed ΔE_{TQ} is significantly smaller than the ΔE_{ST} for these isomers. Also, a large ΔE_{TQ} is observed for the **S1–S2** and **S5–S6** isomers, showing no population (P_Q = 0.0 %) of the $S = 2$ state at room temperature (see Table 2). However, in the cases of the **S3–S4** and **S7–S8** isomers, significantly reduced ΔE_{TQ} is observed (P_Q = 100 %), indicating a thermally accessible $S = 2$ excited state.

MO diagrams of the parent isomers indicate the HOMOs are mostly delocalized along the whole backbones, with a major contribution to the *s*-indacene core (Fig. S12). On the other hand, the LUMOs are mainly localized at the *s*-indacene core. This indicates a large overlap between the frontier MOs of the parent isomers and a closed-shell configuration, which is indicated by the polyradical index ($y_i = 0$). As a result, a large ΔE_{ST} and ΔE_{TQ} are observed (Table 2). Although the HOMOs of the *syn*- and *anti*-isomers have the same delocalization as the parent isomers, clearly, the LUMOs are localized at the two ends of the isomers (Fig. S13–S14). Therefore, charge transfer would occur from the *s*-indacene core to the outer 6,6-dicyanofulvene group. In the cases of the *linear*-isomers at the singlet ($S = 0$) open-shell state, both the α- and β-singly occupied MOs (SOMOs) are localized at the two opposite ends of the molecules (Fig. S15–S18), an indication of a disjoint character of the MOs. Therefore, the π-covalency between the unpaired electrons is reduced, developing open-shell polyradical character (Table 2). Also, the LUMOs of the open-shell molecules are segregated from the SOMOs, which would be beneficial for charge separation. The localization of the α- and β-SOMOs at the opposite ends reduces the electron–electron repulsion, therefore, reducing the ΔE_{ST} gap of the *linear*-isomers. For the $S = 2$ state, SOMO and SOMO−1 are delocalized along the whole backbones, whereas, the SOMO−2 and SOMO−3 are mostly localized at the two ends (Fig. S19–S22). The spin density distributions of the open-shell molecules at the $S = 2$ state indicate the unpaired spins are localized at the two opposite ends (Fig. 5), reducing the ΔE_{TQ} gap of the open-shell isomers and stabilizing $S = 2$ state as a ground-state for the *linear*-isomers. Calculation of the most probable locations of the unpaired electrons indicates major spin contribution is on the two carbon atoms of the carbonaceous rings (Fig. S23), which is consistent with the tetraradical canonical form (see Fig. 3iv). Although, the open-shell molecules show end localized spin density, installation of large and branched alkyl chains should protect the reactive sites.[95]

3.4 Open-shell polyradical character

The prerequisite of high-spin polyradicals is the generation of multiple unpaired electrons in a molecule. A large polyradical character ($y_i \approx 1.0$) is an indication of diminished bond covalency and reduced electron–electron coupling, required to develop high-spin molecules.[16,18,21] As we can see from Table

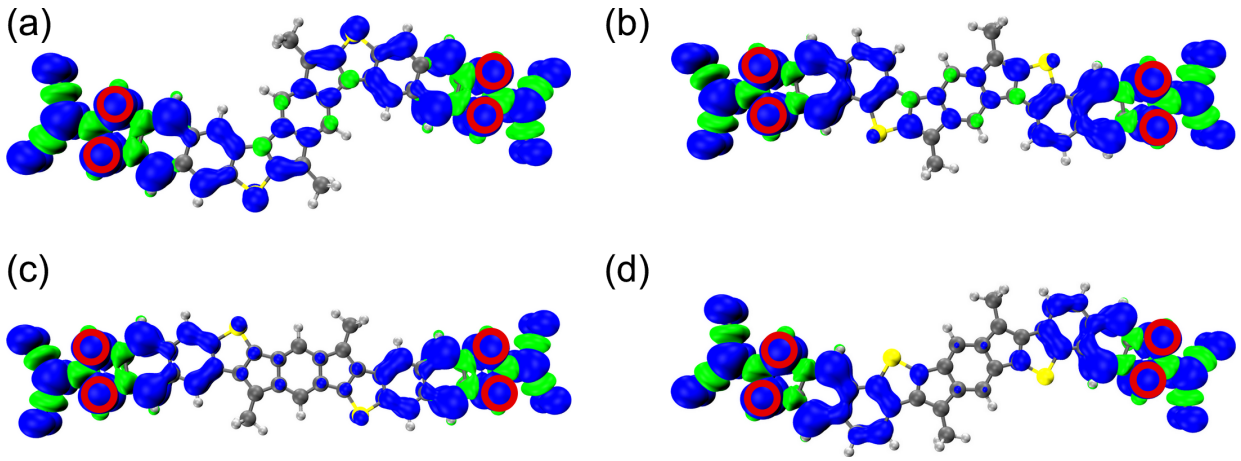

Fig. 5 Spin density distribution of (a) **S9**, (b) **S10**, (c) **S11**, and (d) **S12** at the $S = 2$ state computed with UB3LYP/6-31G(d,p) level of theory and basis set. The blue and green surfaces represent the positive and negative contributions at an isovalue $= 0.001$ a.u., respectively. The most probable locations of the unpaired electrons are highlighted with red (spin-up) open circles.

2, only the *linear*-isomers (**S9**–**S12**) show open-shell polyradical character, not observed for the parent (**1**–**4**), *syn*- (**S1**–**S4**), and *anti*-isomers (**S5**–**S8**). The fractional occupation number weighted electron density (N_{FOD}) indicate the parent isomers should possess an open-shell character, as indicated by the N_{FOD} number, which is close to 2.0. The PUHF calculation shows the parent isomers possess a small open-shell diradical (y_0) character (see Table S1). Extension of the π-conjugation lengths by the addition of 6,6-dicyanofulvene group increases the N_{FOD} number, the largest values observed in the *linear*-isomers (Table 2). The PUHF calculation on the *syn*- and *anti*-isomers indicates an increased open-shell diradical character than their counterpart parent molecules (Table S1), due to the π-extension of the molecular backbone. Also, a very small polyradical character is predicted with the PUHF method for the *syn*- and *anti*-isomers, in line with the N_{FOD} numbers (Table 2 and Table S1). However, there is no open-shell character predicted with the DFT method for the parent, *syn*- and *anti*-isomers. This indicates the parent, *syn*- and *anti*-isomers have mostly closed-shell quinoidal configurations, where the open-shell form is in resonance with the closed-shell structure.[27] The FOD plots (Fig. S24–S27) indicate the parent, *syn*-, and *anti*-isomers have a localized electron density, whereas, the *linear*-isomers have a delocalized density, an indication of open-shell polyradical character.[50,89]

Adding the 6,6-dicyanofulvene group downshift the HOMO and LUMO energy levels from the parent isomers by 0.48–0.79 eV and 0.70–1.23 eV, respectively. As a result, a significant reduction in the HOMO–LUMO energy gap is observed for the *syn*-, *anti*-, and *linear*-isomers than the parent isomers. However, the largest reduction is observed for the *linear*-isomers than the *syn*- and *anti*-isomers. Such as, the calculated HOMO–LUMO energy gap of the parent molecule **2** is 1.85 eV (Table 2). In the cases of the *syn*- (**S2**) and *anti*-isomers (**S6**), this varies between 1.41–1.42 eV, whereas, the *linear*-isomer **S10** shows a HOMO–LUMO energy gap of 1.35 eV. This is the smallest HOMO–LUMO energy gap reported for molecules with *s*-indacene core.[32,34] This small HOMO–LUMO energy gap facilitates admixing the frontier molecular orbitals into the ground-state, generating open-shell polyradical character in the *linear*-isomers. It is well established that molecules with a large antiaromatic character tend to reduce the HOMO–LUMO energy gap.[32,96] We have utilized the NICS-XY scan and 2D-ICSS maps to compare the aromatic/antiaromatic character of the parent and designed molecules. The isomer **1** has the largest antiaromatic core, followed by the *s*-indacene molecule (Fig. 6), in line with the recent report.[32] However, all the designed isomers have a less antiaromatic core than their corresponding parent molecules (See Fig. S28). In the cases of the *syn*- and *anti*-isomers, the outside rings have a similar antiaromatic character as the *s*-indacene core (Fig. 6 and Fig. S28), corroborating their closed-shell configurations. Also, the NICS-XY scan predicts three different regions of varying aromaticity and antiaromaticity, not observed in the parent and *linear*-isomers. These different regions are also visible in the 2D-ICSS maps as well (Fig. S29–S32).

The *linear*-isomers display a very high open-shell diradical character. Such as **S9** shows the largest open-shell diradical character ($y_0 = 0.986$), whereas **S12** possesses the smallest diradical character ($y_0 = 0.928$) among the molecules. This trend is reflected with the PUHF method as well (see Table S1), where the predicted diradical character ($y_0 = 0.986$) is the largest in the **S9** isomer. In the cases of the **S9** and **S10** isomers, a small hexaradical ($y_2 = 0.122$ and 0.111, respectively) character is observed, not predicted for the **S11** and **S12** isomers (Table 2). Both **S11** and **S12** isomers have a large tetraradical character ($y_1 = 0.871$ and 0.800, respectively), which is consistent with their large ΔE_{TQ} energy gap. Recovery of aromatic stabilization energy on the outer benzenoid rings develops open-shell polyradical character for the *linear*-isomers. The NICS-XY scan indicates the core of the **S9** isomer shows increased antiaromaticity than the other open-shell molecules (Fig. 6 and Fig. S28d), however, the outer benzenoid rings have a similar increased aromaticity ($\mathrm{NICS}_{\mathrm{ZZ}} = -14$ to -17 ppm). On the other hand, the *syn*-, and *anti*-isomers have a large antiaromatic character on the outer rings, indicating a closed-shell configuration (Fig. S33–S36). The ACID plots indicate the

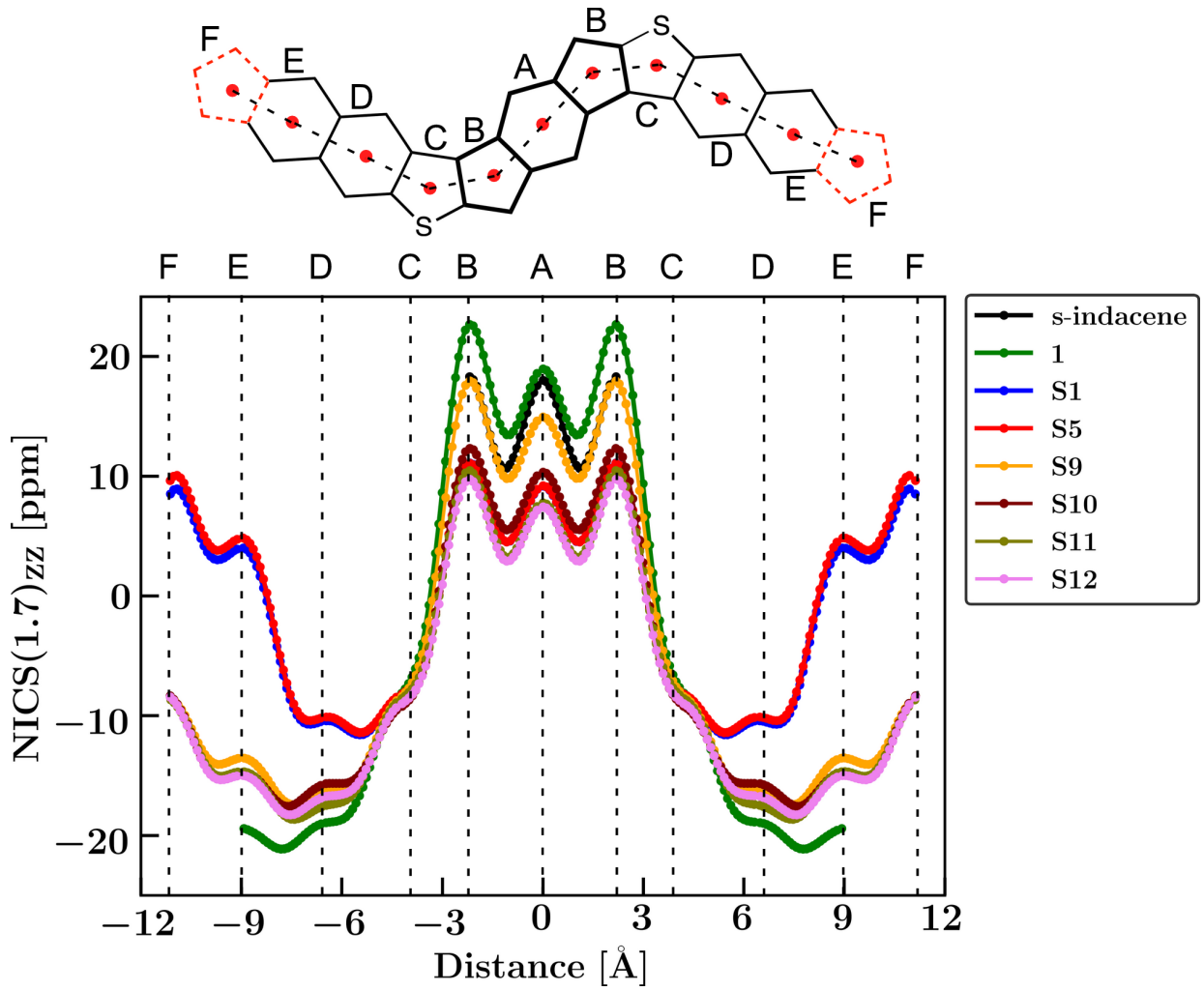

Fig. 6 NICS-XY scan values of *s*-indacene (black), **1** (green), **S1** (blue), **S5** (red), **S9** (gold), **S10** (purple), **S11** (olive), and **S12** (violet). NICS-XY calculation is performed by connecting the geometric centres of the individual rings along the molecular backbone at (U)B3LYP/6-31G(d,p) level of theory and basis set.

parent isomers have a diatropic current density at the outer benzenoid rings and a clear paratropic current at the *s*-indacene core (Fig. S37), which is in line with the BLA, HOMA values, NICS-XY scan, $NICS_{ZZ}(1.7)$ values, and 2D-ICSS maps. This paratropic current density is also visible at the core for the *syn*-, *anti*-, and *linear*-isomers (Fig. 7 and Fig. S38–S39), indicating a large antiaromatic character of the *s*-indacene. In the cases of the open-shell polyradicals, the outer benzenoid rings show a clear diatropic global ring current (Fig. 7). Therefore, many aromatic sextet rings are recovered in the cases of the **S9**–**S12** isomers than the other molecules, increasing the open-shell polyradical character for the *linear*-isomers. A large polyradical character decouples and localizes the unpaired electrons on individual sites (Fig. 3iv and 5, Fig. S23), resulting in a higher degree of electronic coherence. Therefore, a parallel arrangements of the unpaired electrons reduces electron–electron repulsions and stabilize high-spin $S = 2$ ground-state.[16,18,44]

4 Conclusions

We report *s*-indacene core containing indacenodinaphthothiophene isomers with a high-spin quintet ($S = 2$) ground state. Substitution of the strong electron accepting 6,6-dicyanofulvene group at the two ends changes the aromatic character along the conjugated backbone of the *linear*-isomers. Recovery of the aromatic stabilization energy on the outer benzenoid rings provides the necessary potential for double bond breaking, generating open-shell polyradical character. Also, the addition of the 6,6-dicyanofulvene group downshifted both HOMO and LUMO energy levels. The most significant reduction is observed for the *linear*-isomers. As a result, the HOMO–LUMO energy gap is reduced for the *linear*-isomers than the other molecules. A smaller HOMO–LUMO energy gap facilitates admixing of the frontier orbitals into the ground state, generating open-shell polyradical character. A large polyradical character indicates the localization of the unpaired electrons into individual sites, diminishing the bond covalency and reducing electron–electron repulsions. As a result, parallel alignment of the unpaired electrons reduces

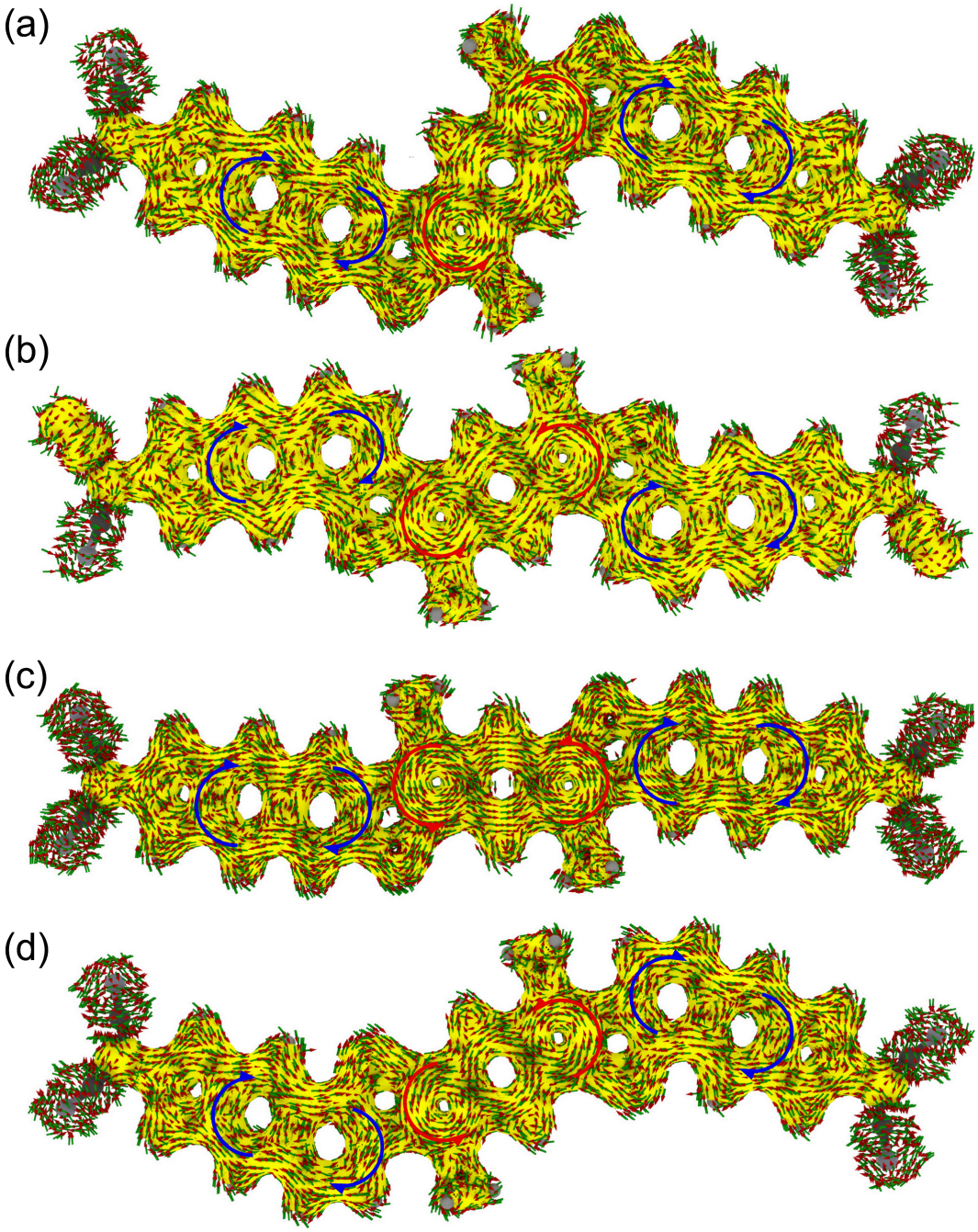

Fig. 7 ACID plots for (a) **S9**, (b) **S10**, (c) **S11**, and (d) **S12** at the $S = 2$ state. The clockwise (diatropic: aromatic) and counterclockwise (paratropic: antiaromatic) ring currents are indicated by blue and red arrows, respectively. The applied magnetic field is perpendicular to the molecular backbone and pointed out through the molecule plane. ACID plots generated with an isovalue = 0.015 a.u.

the energy, stabilizing the high-spin $S = 2$ ground-state. A large ΔE_{TQ} inherent to these molecules show an exclusive population of the $S = 2$ state at room temperature. However, the *syn*- and *anti*-isomers have an extensive antiaromatic backbone and show a closed-shell low-spin singlet ground state. Our design strategy indicates easy tuning of molecular topology to develop novel materials with a high-spin quintet ground-state, which are potential candidates for spintronic and room-temperature magnetic applications.

5 Conflicts of interest

No conflicts of interest to declare.

6 Acknowledgements

This work is supported by the National Science Foundation (NSF) under grant no. OIA-1757220. The DFT calculations were performed at the high-performance computing center at Mississippi State University. Also, the Extreme Science and Engineering Discovery Environment (XSEDE)[97] was used, which is supported by NSF grant number ACI-1548562. We acknowledge the Texas Ad-

vanced Computing Center (TACC) at the University of Texas at Austin for providing (HPC, Stampede 2 (through XSEDE allocation, TG-CHE140141)) resources that have contributed to the research results reported within this paper. We thank to an anonymous reviewer for helpful comments to improve the quality of our work.

Notes and references

1 A. Rajca, *Chem. Rev.*, 1994, **94**, 871–893.

2 A. Rajca, *Adv. Phys. Org. Chem.*, 2005, **40**, 153–199.

3 S. Sanvito, *Chem. Soc. Rev.*, 2011, **40**, 3336–3355.

4 T. Sugawara, H. Komatsu and K. Suzuki, *Chem. Soc. Rev.*, 2011, **40**, 3105–3118.

5 T. Y. Gopalakrishna, W. Zeng, X. Lu and J. Wu, *ChemComm.*, 2018, **54**, 2186–2199.

6 D. A. Dougherty, *Acc. Chem. Res.*, 1991, **24**, 88–94.

7 N. M. Gallagher, A. Olankitwanit and A. Rajca, *J. Org. Chem.*, 2015, **80**, 1291–1298.

8 W. M. Nau, *Angew. Chem. Int. Ed. Eng.*, 1997, **36**, 2445–2448.

9 A. Rajca, *J. Am. Chem. Soc.*, 1990, **112**, 5890–5892.

10 A. Rajca, S. Rajca and S. R. Desai, *J. Am. Chem. Soc.*, 1995, **117**, 806–816.

11 A. Rajca, A. Olankitwanit, Y. Wang, P. J. Boratynski, M. Pink and S. Rajca, *J. Am. Chem. Soc.*, 2013, **135**, 18205–18215.

12 A. Rajca, J. Wongsriratanakul and S. Rajca, *Science*, 2001, **294**, 1503–1505.

13 A. E. London, L. Huang, B. A. Zhang, M. B. Oviedo, J. Tropp, W. Yao, Z. Wu, B. M. Wong, T. N. Ng and J. D. Azoulay, *Polym. Chem.*, 2017, **8**, 2922–2930.

14 Y. Joo, L. Huang, N. Eedugurala, A. E. London, A. Kumar, B. M. Wong, B. W. Boudouris and J. D. Azoulay, *Macromolecules*, 2018, **51**, 3886–3894.

15 D. B. Sulas, A. E. London, L. Huang, L. Xu, Z. Wu, T. N. Ng, B. M. Wong, C. W. Schlenker, J. D. Azoulay and M. Y. Sfeir, *Adv. Opt. Mater.*, 2018, **6**, 1701138.

16 A. E. London, H. Chen, M. Sabuj, J. Tropp, M. Saghayezhian, N. Eedugurala, B. Zhang, Y. Liu, X. Gu, B. Wong, N. Rai and J. Azoulay, *Sci. Adv.*, 2019, **5**, eaav2336.

17 K. Wang, L. Huang, N. Eedugurala, S. Zhang, M. A. Sabuj, N. Rai, X. Gu, J. D. Azoulay and T. N. Ng, *Adv. Energy Mater.*, 2019, **9**, 1902806.

18 M. A. Sabuj, M. M. Huda, C. S. Sarap and N. Rai, *Mater. Adv.*, 2021, **2**, 2943–2955.

19 M. A. Sabuj, *Organic Open-Shell Materials for Optoelectronic and Magnetic Applications*, Mississippi State University, 2020.

20 T. L. D. Tam, G. Wu, S. W. Chien, S. F. V. Lim, S.-W. Yang and J. Xu, *ACS Mater. Lett.*, 2020, **2**, 147–152.

21 M. Steelman, D. J. Adams, K. S. Mayer, P. Mahalingavelar, C.-T. Liu, N. Eedugurala, M. Lockart, Y. Wang, X. Gu, M. K. Bowman and J. D. Azoulay, *Adv. Mater.*, 2022, 2206161.

22 M. A. Sabuj, O. Muoh, M. M. Huda and N. Rai, *Phys. Chem. Chem. Phys.*, 2022, **24**, 23699–23711.

23 J. Thiele and H. Balhorn, *Ber. Dtsch. Chem. Ges.*, 1904, **37**, 1463–1470.

24 A. Tschitschibabin, *Ber. Dtsch. Chem. Ges.*, 1907, **40**, 1810–1819.

25 M. Bendikov, H. M. Duong, K. Starkey, K. Houk, E. A. Carter and F. Wudl, *J. Am. Chem. Soc.*, 2004, **126**, 7416–7417.

26 P. Karafiloglou, *J. Chem. Educ.*, 1989, **66**, 816.

27 G. E. Rudebusch, J. L. Zafra, K. Jorner, K. Fukuda, J. L. Marshall, I. Arrechea-Marcos, G. L. Espejo, R. P. Ortiz, C. J. Gómez-García and L. N. Zakharov, *Nat. Chem.*, 2016, **8**, 753–759.

28 J. J. Dressler, M. Teraoka, G. L. Espejo, R. Kishi, S. Takamuku, C. J. Gómez-García, L. N. Zakharov, M. Nakano, J. Casado and M. M. Haley, *Nat. Chem.*, 2018, **10**, 1134–1140.

29 J. J. Dressler, A. C. Valdivia, R. Kishi, G. E. Rudebusch, A. M. Ventura, B. E. Chastain, C. J. Gómez-García, L. N. Zakharov, M. Nakano and J. Casado, *Chem*, 2020, **6**, 1353–1368.

30 J. L. Marshall, K. Uchida, C. K. Frederickson, C. Schütt, A. M. Zeidell, K. P. Goetz, T. W. Finn, K. Jarolimek, L. N. Zakharov and C. Risko, *Chem. Sci.*, 2016, **7**, 5547–5558.

31 C. K. Frederickson, L. N. Zakharov and M. M. Haley, *J. Am. Chem. Soc.*, 2016, **138**, 16827–16838.

32 G. I. Warren, J. E. Barker, L. N. Zakharov and M. M. Haley, *Org. Lett.*, 2021, **23**, 5012–5017.

33 J. E. Barker, J. J. Dressler, A. Cardenas Valdivia, R. Kishi, E. T. Strand, L. N. Zakharov, S. N. MacMillan, C. J. Gomez-Garcia, M. Nakano and J. Casado, *J. Am. Chem. Soc.*, 2019, **142**, 1548–1555.

34 J. E. Barker, T. W. Price, L. J. Karas, R. Kishi, S. N. MacMillan, L. N. Zakharov, C. J. Gómez-García, J. I. Wu, M. Nakano and M. M. Haley, *Angew. Chem.*, 2021, **133**, 22559–22566.

35 J. J. Dressler, J. E. Barker, L. J. Karas, H. E. Hashimoto, R. Kishi, L. N. Zakharov, S. N. MacMillan, C. J. Gomez-Garcia, M. Nakano and J. I. Wu, *J. Org. Chem.*, 2020, **85**, 10846–10857.

36 Z. Zeng, X. Shi, C. Chi, J. T. L. Navarrete, J. Casado and J. Wu, *Chem. Soc. Rev.*, 2015, **44**, 6578–6596.

37 T. Kubo, *Chem. Lett.*, 2015, **44**, 111–122.

38 Z. Sun, Z. Zeng and J. Wu, *Acc. Chem. Res.*, 2014, **47**, 2582–2591.

39 T. Kubo, A. Shimizu, M. Sakamoto, M. Uruichi, K. Yakushi, M. Nakano, D. Shiomi, K. Sato, T. Takui and Y. Morita, *Angew. Chem. Int. Ed.*, 2005, **44**, 6564–6568.

40 C. K. Frederickson, B. D. Rose and M. M. Haley, *Acc. Chem. Res.*, 2017, **50**, 977–987.

41 H. Miyoshi, M. Miki, S. Hirano, A. Shimizu, R. Kishi, K. Fukuda, D. Shiomi, K. Sato, T. Takui and I. Hisaki, *J. Org. Chem.*, 2017, **82**, 1380–1388.

42 P. Hu and J. Wu, *Can. J. Chem.*, 2017, **95**, 223–233.

43 Z.-Y. Wang, Y.-Z. Dai, L. Ding, B.-W. Dong, S.-D. Jiang, J.-Y. Wang and J. Pei, *Angew. Chem. Int. Ed.*, 2021, **60**, 4594–4598.

44 A. Shimizu, T. Morikoshi, K. Sugisaki, D. Shiomi, K. Sato, T. Takui and R. Shintani, *Angew. Chem. Int. Ed.*, 2022, **61**, e202205729.

45 M. Nendel, B. Goldfuss, K. Houk and K. Hafner, *J. Mol. Struct.: THEOCHEM*, 1999, **461**, 23–28.

46 K. Hafner, B. Stowasser, H.-P. Krimmer, S. Fischer, M. C. Böhm and H. J. Lindner, *Angew. Chem. Int. Ed. Engl. 1986,*, 1986, **25**, 630–632.

47 B. S. Young, D. T. Chase, J. L. Marshall, C. L. Vonnegut, L. N. Zakharov and M. M. Haley, *Chem. Sci.*, 2014, **5**, 1008–1014.

48 A. Shimizu, R. Kishi, M. Nakano, D. Shiomi, K. Sato, T. Takui, I. Hisaki, M. Miyata and Y. Tobe, *Angew. Chem. Int. Ed.*, 2013, **125**, 6192–6195.

49 T. Xu, Y. Han, Z. Shen, X. Hou, Q. Jiang, W. Zeng, P. W. Ng and C. Chi, *J. Am. Chem. Soc.*, 2021, **143**, 20562–20568.

50 Z. Chen, W. Li, M. A. Sabuj, Y. Li, W. Zhu, M. Zeng, C. S. Sarap, M. M. Huda, X. Qiao, X. Peng and N. Rai, *Nat. Commun.*, 2021, **12**, 1–10.

51 M. Abe, *Chem. Rev.*, 2013, **113**, 7011–7088.

52 M. Nakano, R. Kishi, A. Takebe, M. Nate, H. Takahashi, T. Kubo, K. Kamada, K. Ohta, B. Champagne and E. Botek, *CoLe*, 2007, **3**, 333–338.

53 K. Yang, X. Zhang, A. Harbuzaru, L. Wang, Y. Wang, C. Koh, H. Guo, Y. Shi, J. Chen and H. Sun, *J. Am. Chem. Soc.*, 2020, **142**, 4329–4340.

54 T. Takahashi, K.-i. Matsuoka, K. Takimiya, T. Otsubo and Y. Aso, *J. Am. Chem. Soc.*, 2005, **127**, 8928–8929.

55 R. Ponce Ortiz, J. Casado, S. Rodriguez Gonzalez, V. Hernández, J. T. Lopez Navarrete, P. M. Viruela, E. Ortí, K. Takimiya and T. Otsubo, *Chem. Eur. J.*, 2010, **16**, 470–484.

56 T. Ullrich, D. Munz and D. M. Guldi, *Chem. Soc. Rev.*, 2021, **50**, 3485.

57 Z. Lin, L. Chen, Q. Xu, G. Shao, Z. Zeng, D. Wu and J. Xia, *Org. lett.*, 2020, **22**, 2553–2558.

58 G. E. Rudebusch, A. G. Fix, H. A. Henthorn, C. L. Vonnegut, L. N. Zakharov and M. M. Haley, *Chem. Sci.*, 2014, **5**, 3627–3633.

59 J. Casado, R. P. Ortiz and J. T. L. Navarrete, *Chem. Soc. Rev.*, 2012, **41**, 5672–5686.

60 C. Liu, M. E. Sandoval-Salinas, Y. Hong, T. Y. Gopalakrishna, H. Phan, N. Aratani, T. S. Herng, J. Ding, H. Yamada, D. Kim, D. Casanova and J. Wu, *Chem*, 2018, **4**, 1586–1595.

61 S. Nobusue, H. Miyoshi, A. Shimizu, I. Hisaki, K. Fukuda, M. Nakano and Y. Tobe, *Angew. Chem. Int. Ed.*, 2015, **54**, 2090–2094.

62 X. Lu, S. Lee, J. O. Kim, T. Y. Gopalakrishna, H. Phan, T. S. Herng, Z. Lim, Z. Zeng, J. Ding, D. Kim and J. Wu, *J. Am. Chem. Soc.*, 2016, **138**, 13048–13058.

63 X. Lu, S. Lee, Y. Hong, H. Phan, T. Y. Gopalakrishna, T. S. Herng, T. Tanaka, M. E. Sandoval-Salinas, W. Zeng, J. Ding, D. Kim, D. Casanova and J. Wu, *J. Am. Chem. Soc.*, 2017, **139**, 13173–13183.

64 P. Hu, S. Lee, T. S. Herng, N. Aratani, T. P. Gonçalves, Q. Qi, X. Shi, H. Yamada, K.-W. Huang, J. Ding and J. Wu, *J. Am. Chem. Soc.*, 2016, **138**, 1065–1077.

65 M. A. Sabuj and N. Rai, *Mol. Syst. Des. Eng.*, 2020, **5**, 1477–1490.

66 T. Stuyver, B. Chen, T. Zeng, P. Geerlings, F. De Proft and R. Hoffmann, *Chem. Rev.*, 2019, **119**, 11291–11351.

67 H. Hayashi, J. E. Barker, A. Cardenas Valdivia, R. Kishi, S. N. MacMillan, C. J. Gómez-García, H. Miyauchi, Y. Nakamura, M. Nakano and S.-i. Kato, *J. Am. Chem. Soc.*, 2020, **142**, 20444–20455.

68 M. A. Sabuj, M. M. Huda and N. Rai, *iScience*, 2020, **23**, 101675.

69 A. Das, T. Muller, F. Plasser and H. Lischka, *J. Phys. Chem. A*, 2016, **120**, 1625–1636.

70 P. Rivero, C. A. Jimenez-Hoyos and G. E. Scuseria, *J. Phys. Chem. B*, 2013, **117**, 12750–12758.

71 C. Liu, Y. Ni, X. Lu, G. Li and J. Wu, *Acc. Chem. Res.*, 2019, **52**, 2309–2321.

72 S. Das, T. S. Herng, J. L. Zafra, P. M. Burrezo, M. Kitano, M. Ishida, T. Y. Gopalakrishna, P. Hu, A. Osuka, J. Casado, D. Casanova and J. Wu, *J. Am. Chem. Soc.*, 2016, **138**, 7782–7790.

73 G. Li, Y. Han, Y. Zou, J. J. C. Lee, Y. Ni and J. Wu, *Angew. Chem.*, 2019, **131**, 14457–14464.

74 M. J. Frisch, G. W. Trucks, H. B. Schlegel, G. E. Scuseria, M. A. Robb, J. R. Cheeseman, G. Scalmani, V. Barone, G. A. Petersson, H. Nakatsuji, X. Li, M. Caricato, A. V. Marenich, J. Bloino, B. G. Janesko, R. Gomperts, B. Mennucci, H. P. Hratchian, J. V. Ortiz, A. F. Izmaylov, J. L. Sonnenberg, D. Williams-Young, F. Ding, F. Lipparini, F. Egidi, J. Goings, B. Peng, A. Petrone, T. Henderson, D. Ranasinghe, V. G. Zakrzewski, J. Gao, N. Rega, G. Zheng, W. Liang, M. Hada, M. Ehara, K. Toyota, R. Fukuda, J. Hasegawa, M. Ishida, T. Nakajima, Y. Honda, O. Kitao, H. Nakai, T. Vreven, K. Throssell, J. A. Montgomery, Jr., J. E. Peralta, F. Ogliaro, M. J. Bearpark, J. J. Heyd, E. N. Brothers, K. N. Kudin, V. N. Staroverov, T. A. Keith, R. Kobayashi, J. Normand, K. Raghavachari, A. P. Rendell, J. C. Burant, S. S. Iyengar, J. Tomasi, M. Cossi, J. M. Millam, M. Klene, C. Adamo, R. Cammi, J. W. Ochterski, R. L. Martin, K. Morokuma, O. Farkas, J. B. Foresman and D. J. Fox, *Gaussian 16 Revision B.01*, 2016, Gaussian Inc. Wallingford CT.

75 A. D. Becke, *J. Chem. Phys.*, 1993, **98**, 1372–1377.

76 P. Stephens, F. Devlin, C. Chabalowski and M. J. Frisch, *J. Phys. Chem.*, 1994, **98**, 11623–11627.

77 M. M. Francl, W. J. Pietro, W. J. Hehre, J. S. Binkley, M. S. Gordon, D. J. DeFrees and J. A. Pople, *J. Chem. Phys.*, 1982, **77**, 3654–3665.

78 A. Konishi, K. Horii, D. Shiomi, K. Sato, T. Takui and M. Yasuda, *J. Am. Chem. Soc.*, 2019, **141**, 10165–10170.

79 J. M. Herbert, *arXiv preprint arXiv:2204.10135*, 2022.

80 L. Noodleman, *J. Chem. Phys.*, 1981, **74**, 5737–5743.

81 E. D. Glendening, C. R. Landis and F. Weinhold, *J. Comput. Chem.*, 2013, **34**, 1429–1437.

82 P. v. R. Schleyer, M. Manoharan, Z.-X. Wang, B. Kiran, H. Jiao, R. Puchta and N. J. van Eikema Hommes, *Org. Lett.*, 2001, **3**, 2465–2468.

83 R. Gershoni-Poranne and A. Stanger, *Chem.: Eur. J.*, 2014, **20**, 5673–5688.

84 R. Ditchfield, *Mol. Phys.*, 1974, **27**, 789–807.

85 R. Herges and D. Geuenich, *J. Phys. Chem. A*, 2001, **105**, 3214–3220.
86 T. A. Keith and R. F. Bader, *Chem. Phys. Lett.*, 1993, **210**, 223–231.
87 S. Klod and E. Kleinpeter, *J. Chem. Soc., Perkin. Trans. 2*, 2001, 1893–1898.
88 S. Grimme and A. Hansen, *Angew. Chem. Int. Ed.*, 2015, **54**, 12308–12313.
89 F. Neese, *Wiley Interdiscip. Rev.: Comput. Mol. Sci.*, 2012, **2**, 73–78.
90 J. Kruszewski and T. Krygowski, *Tetrahedron Lett.*, 1972, **13**, 3839–3842.
91 T. M. Krygowski and M. K. Cyrański, *Chem. Rev.*, 2001, **101**, 1385–1420.
92 W. Humphrey, A. Dalke and K. Schulten, *J. Molec. Graphics*, 1996, **14**, 33–38.
93 T. Yanai, D. P. Tew and N. C. Handy, *Chem. Phys. Lett.*, 2004, **393**, 51–57.
94 J.-D. Chai and M. Head-Gordon, *Phys. Chem. Chem. Phys.*, 2008, **10**, 6615–6620.
95 Z. Zeng, S. Lee, J. L. Zafra, M. Ishida, N. Bao, R. D. Webster, J. T. L. Navarrete, J. Ding, J. Casado, D. Kim *et al.*, *Chem. Sci.*, 2014, **5**, 3072–3080.
96 M. Schmidt, D. Wassy, M. Hermann, M. T. González, N. Agräit, L. A. Zotti, B. Esser and E. Leary, *Chem. Commun.*, 2021, **57**, 745–748.
97 J. Towns, T. Cockerill, M. Dahan, I. Foster, K. Gaither, A. Grimshaw, V. Hazlewood, S. Lathrop, D. Lifka and G. D. Peterson, *Comput. Sci. Eng.*, 2014, **16**, 62–74.